



HAL
open science

Iron Isotope Fractionation during Bio- and Photodegradation of Organoferric Colloids in Boreal Humic Waters

Olga Oleinikova, Franck Poitrasson, Olga Yu. Drozdova, Liudmila Shirokova,
Sergey Lapitskiy, Oleg Pokrovsky

► **To cite this version:**

Olga Oleinikova, Franck Poitrasson, Olga Yu. Drozdova, Liudmila Shirokova, Sergey Lapitskiy, et al.. Iron Isotope Fractionation during Bio- and Photodegradation of Organoferric Colloids in Boreal Humic Waters. *Environmental Science and Technology*, 2019, 53 (19), pp.11183-11194. 10.1021/acs.est.9b02797 . hal-02399037v1

HAL Id: hal-02399037

<https://hal.science/hal-02399037v1>

Submitted on 19 Nov 2020 (v1), last revised 30 Sep 2021 (v2)

HAL is a multi-disciplinary open access archive for the deposit and dissemination of scientific research documents, whether they are published or not. The documents may come from teaching and research institutions in France or abroad, or from public or private research centers.

L'archive ouverte pluridisciplinaire **HAL**, est destinée au dépôt et à la diffusion de documents scientifiques de niveau recherche, publiés ou non, émanant des établissements d'enseignement et de recherche français ou étrangers, des laboratoires publics ou privés.

1 Iron isotope fractionation during bio- and photo-degradation
2 of organo-ferric colloids in boreal humic waters

3
4 Olga V. OLENIKOVA¹, Franck POITRASSON¹, Olga Yu. DROZDOVA², Liudmila S. SHIROKOVA^{1,3},
5 Sergey A. LAPITSKIY², and Oleg S. POKROVSKY^{1,3,4*}

6
7 ¹ GET (Geosciences and Environment Toulouse) UMR 5563 CNRS, 14 Avenue Edouard Belin,
8 31400 Toulouse, France

9 ² Geological Faculty of Moscow State University, 1 Leninskie Gory, 119234 Moscow, Russia

10 ³ N. Laverov Federal Center for Integrated Arctic Research, Russian Academy of Science,
11 Arkhangelsk, Russia

12 ⁴ BIO-GEO-CLIM Laboratory, Tomsk State University, 36 Lenina av., 634050 Tomsk, Russia

13
14 * Corresponding author. *Email address:* oleg.pokrovsky@get.omp.eu (Oleg S. Pokrovsky).

15
16
17 Key words: Fe, heterotrophic bacteria, photolysis, sunlight, Arctic, organic carbon, complexation,
18 size fractionation, oxidation, precipitation

19
20
21
22 Submitted to *Environ Sci Technol* after revision, May 2019

23
24
25 Key messages:

26 Adsorption of heavy Fe isotopes on heterotrophic bacteria cell surface

27 Assimilation of light Fe isotopes by live *P. aureofaciens* cells

28 Removal of heavy Fe isotopes from solution during sunlight oxidation of organo-ferric colloids

29 Generation of isotopically light Fe(II) in LMW_{< 1 kDa} during photolysis

30 Bio- and photodegradation of organo-ferric colloids can produce very large, from -2.5 to +3.2‰

31 $\delta^{57}\text{Fe}$ isotopic variations in boreal waters

41 ABSTRACT

42 Bio-degradation and photolysis of dissolved organic matter (DOM) in boreal high-latitude waters
43 are the **two** main factors controlling **aquatic fluxes and residence time** of carbon **but also metal** nutrients
44 associated with DOM such as Fe. **The DOM is usually present in the form of organic and organo-**
45 **mineral colloids that also account for the majority of dissolved Fe.** Here we use the stable Fe isotope
46 approach to unravel the processes controlling Fe behavior during bio- and photo-**degradation of**
47 **colloids in** boreal **Fe- and DOM-rich humic waters (a stream and a fen).** The adsorption of Fe colloids
48 onto heterotrophic bacteria *P. aureofaciens* produced enrichment in +0.4‰ (**$\delta^{57}\text{Fe}$**) in the heavier
49 isotopes of the cell surface relative to the remaining solution. **In contrast, long-term assimilation of Fe**
50 **by live cells yielded preferential incorporation of lighter isotopes into the cells (-0.7‰ relative to**
51 **aqueous solution).** The sunlight-induced oxidation of Fe(II) in **fen** water and coagulation of organo-
52 ferric colloids led to removal of heavier Fe isotopes (**+1.5 to +2.5‰**) from **solution**, consistent with
53 Fe(III) hydroxide precipitation from Fe(II)-bearing solution. Altogether, bio- and photodegradation of
54 organo-ferric colloids, occurring within a few days of exposure time, can produce several **per mil**
55 isotopic excursions in shallow lentic and lotic inland waters of high latitude boreal regions.
56 **Considerable** daily scale variations of Fe isotopic **composition** should therefore be taken into account
57 during interpretation of riverine flux of Fe isotope to the ocean or tracing weathering processes using
58 Fe isotopes in surface waters at high latitudes.

59

60 1. Introduction

61 Despite broad use of Fe isotopes for tracing various large-scale, long-term processes at the
62 **Earth's** surface^{1,2}, notably in river³⁻⁸ or lake^{9,10} waters, **the fractionation of Fe isotopes during short-**
63 **term processes such as bio- and photo-degradation of organic matter that binds Fe in freshwater** remain
64 poorly understood. This is especially true for organic **carbon** and Fe-rich boreal waters, **that, from the**
65 **one hand, play** a primary role in the C cycle, CO₂ emissions and storage¹¹ and from the other hand,
66 **strongly contribute** to Fe and other micro-nutrient export by **rivers** to the **coastal productive zones**^{13,14}.

67 The majority of dissolved (< 0.22 μm) Fe and other metals in boreal waters are present in the
68 form of organic and organo-mineral colloids (1 nm - 0.22 μm) whose transport and bioavailability are
69 dramatically different from inorganic ions or simple organic complexes¹⁵. Two main processes
70 responsible for fluxes and residence time of organic C and metal colloids in boreal high-latitude aquatic
71 environments are heterotrophic bacterial respiration (degradation of DOM) and photolysis¹⁶. Colloidal
72 transformation often occurs along the hydrological continuum of interconnected soil waters, mires,
73 streams and large oligotrophic lakes¹⁷. During this transformation, induced mainly by aquatic
74 microorganisms and sunlight irradiation, the organic and organo-ferric colloids are subjected to *i*)
75 change of dominant source and molecular weight from allochthonous large-size humic and fulvic
76 molecules to small size autochthonous organic ligands¹⁷, *ii*) degradation of DOC into CO₂ or
77 intracellular uptake of DOC by bacterioplankton and liberation of Fe(III) ions, leading to Fe
78 oxy(hydr)oxide precipitation^{18,19}, and *iii*) enrichment in low molecular weight organic ligands and their
79 complexes with metals²⁰.

80 In contrast to numerous works devoted to microbiological²¹ and photochemical²²
81 mineralization of dissolved organic carbon (DOC), nitrogen and phosphorus, the bacterial and
82 sunlight-induced transformations of Fe-rich colloids in inland waters have been little studied^{23,24}. The
83 transformation of colloidal Fe in boreal waters, including bogs, lakes and rivers²⁵ has been studied
84 under the metabolic action of heterotrophic soil and aquatic bacteria^{18,26-27} and sunlight²⁸. In these
85 works we demonstrated that the biodegradation of organo-ferric colloids by heterotrophic bacteria
86 consists of *i*) element uptake inside the cells; *ii*) element adsorption at the cell surface, and *iii*) Fe
87 hydroxide precipitation leading to scavenging of associated trace metals. During both biodegradation
88 and photolysis of natural DOM, Fe plays a pivotal role in controlling the fate of trace elements (TE).
89 This control occurs via *i*) formation of insoluble Fe(III) hydroxides that coprecipitate other trace
90 metals²⁸, and *ii*) generation of low molecular weight (LMW) organic ligands that bind Fe, thus
91 competing with strong organic complexes of other metals^{19,20,28}.

92 The Fe isotope approach is an efficient tool for deciphering elementary processes involving
93 microbes and aqueous solutions²⁹⁻³³, DOM Fe³⁴ and mineral Fe^{35,36} interaction including colloids^{3,6,}
94 ³⁷. The latter study demonstrated an unusual enrichment of heavier Fe isotopes in the LMW (< 1-10
95 kDa) fraction relative to remaining colloidal fraction (by up to +3 to +4 ‰ in $\delta^{57}\text{Fe}$) and suggested
96 that bio- and/or photo-transformation of colloids may be responsible for heavy Fe isotope signatures
97 in LMW fraction of boreal waters. However, the photo-oxidation of organo-ferric colloids removes Fe
98 in the form of Fe(III) hydroxides^{19,23,38} which can enrich the remaining solution in lighter Fe isotopes,
99 consistent with numerous laboratory experiments on Fe hydroxide precipitation from Fe(II)-bearing
100 aqueous solution³⁹. Whereas for $\text{Fe}^{3+}(\text{aq}) \rightarrow \text{Fe(III)}_{\text{solid}}$ (hematite) reaction at equilibrium, a negligible
101 fractionation of -0.15 ± 0.30 ‰ ($\Delta^{57}\text{Fe}$) was reported⁴⁰, the $\text{Fe}^{2+}(\text{aq}) \rightarrow \text{Fe(III)}_{\text{solid}}$ (ferrihydrite) reaction
102 has $\Delta^{57}\text{Fe}$ of $+4.8 \pm 0.15$ ‰³⁹. Other experiments producing goethite reported a fractionation factor of
103 $+1.7 \pm 0.14$ ‰, corresponding to the $\text{Fe(III)}_{\text{solid}}$ being enriched in heavier isotopes⁴¹. As for the
104 bacterially-induced colloid transformation, two main processes controlling the isotope fractionation
105 during metal-live cell interaction are 1) fast adsorption of heavier Fe isotope on the cell surfaces^{30,31},
106 and 2) long-term assimilation of heavier Fe isotopes as recently shown for phytoplankton⁴² and
107 magnetotactic bacteria³³. Note however that, in contrast to the fairly good knowledge of isotope
108 fractionation of ionic metals and their organic complexes interaction with microbial cells, virtually
109 nothing is known on colloidal metal – cell interaction reactions. The present study is aimed at the
110 quantification of Fe isotope signatures during photo- and bio-degradation of DOM-Fe complexes in
111 high latitude boreal waters. We hypothesized preferential removal of heavier Fe isotopes by live cell
112 adsorption and assimilation and Fe hydroxide precipitation in the course of bio- and photodegradation
113 of organo-ferric colloids. We further tested the possibility of formation of isotopically heavy Fe in
114 LMW_{< 1 kDa} fraction of river waters, as it was put forward in a previous study³⁷. To test these
115 hypotheses, we selected a stream and a fen water, two dominant types of Fe-rich freshwaters of the
116 subarctic. By choosing two main processes controlling the fate of organo-ferric colloids (bio- and
117 photo-degradation) and two representative examples of boreal Fe- and DOM-rich surface waters, we

118 were capable to reveal the main factors that govern Fe isotope behavior on a short-term (daily) scale
119 in large territory of subarctic landscapes.

120

121 2. Materials and methods

122 The surface waters were collected in the Northern Karelia region (NW Russia). The climate of
123 the region is mild-cold, transitional between oceanic and continental. Average temperature in
124 January is -13 °C, and +15 °C in July; average annual precipitation ranges between 450 and 550 mm
125 y⁻¹. Our study area is in the most elevated part of Karelia, within a landscape of tectonic denudation
126 hills, plateaus and ridges with an average altitude of 300-400 m, with separate insulated massifs.
127 Predominant soils are illuvial-humic and illuvial-ferruginous-humic podzols. Coniferous forest (pine
128 and spruce) with some deciduous trees (birch, aspen and alder) dominates the vegetation of the
129 region. Further landscape setting is described in previous works of our group^{17,37}. Within the
130 hydrological continuum created by glacial processes around 8-10 thousand years ago, the water and
131 soluble compounds travel from the ombrotrophic peat mire zone downstream the river towards a
132 large oligotrophic lake. At the lake coast, there are minerotrophic fens located in depressions that
133 receive their water via shallow groundwater and soil flux⁴³.

134 A small stream and a coastal fen were collected in July 2015, during summer baseflow period.
135 The Palojoki stream (watershed area = 32 km², bedrock of granites, gneisses, syenites, and syenite-
136 diorites of the early-Proterozoic and late-Archean, covered by glacial Quaternary deposits under
137 podzol soils⁴³) was sampled in the middle course of the flow (sample KAR-1¹⁷). The fen adjacent to
138 the western coast of the Tsipringa Lake had an area of 1.19 km² and is underlain by Early-Archean
139 biotite granito-gneisses (sample ZPBL¹⁷).

140 The experiments included on-site photodegradation of sterile-filtered (< 0.22 μm) stream and
141 fen water in quartz reactors and laboratory microcosm experiments in the presence of 1 g_{wet}/L of
142 *Pseudomonas aureofaciens*, highly abundant culturable bacteria isolated from podzol soils⁴⁴. The
143 experimental scheme described in previous works from our group^{27,28}, is shown in Fig. 1. The

144 biodegradation experiments with stream and fen waters were performed after 6 months storage of
145 sterile-filtered samples in the refrigerator. Freshly-collected bacteria at the stationary growth stage
146 were rinsed in 0.85% NaCl and allowed to starve in nutrient-free 0.85% NaCl solution during 5 days.
147 The cells were rinsed again 3 times before the experiment, concentrated in a mother suspension and
148 added to sterile, acid-washed polypropylene flasks with stream or fen water (typically 2 mL of
149 bacterial suspension to 200 mL of water) to provide the wet biomass concentration of $1 \text{ g}_{\text{wet}} \text{ L}^{-1}$. Note
150 that the amount of Fe originated from bacteria addition does not exceed $1 \mu\text{g L}^{-1}$ for this concentration
151 of biomass²⁷. The flasks were shaken at $25 \pm 0.5^\circ\text{C}$ and aerated via Biosilico® ventilation porous caps
152 during 4 days. Aliquots of homogeneous suspension were sampled after 0, 1, 8, 22, 30, 50 and 100 h
153 after the addition of bacteria and filtered through $0.22 \mu\text{m}$ membrane. All the experiments were run in
154 duplicates. The control experiment was sterile filtered ($< 0.22 \mu\text{m}$) biomass-free stream and fen water
155 and it was processed exactly as bacterial samples.

156 For photo-degradation experiments, the stream and fen waters were collected in pre-cleaned
157 polypropylene jars and stored in dark cold place ($6 \pm 2^\circ\text{C}$) prior the experiments. The waters were
158 processed on-site, within 2 h after sampling, in the field-constructed clean laboratory³⁷. Sterile
159 filtration was performed using single-used Sartorius polystyrene vacuum filtration units ($0.22 \mu\text{m}$, 250
160 mL volume). Filtered fluids were transferred into 270-mL sterilized quartz flasks, filled with 10% air
161 headspace and covered by porous sterile stoppers. The dark control of quartz flasks was identical to
162 the light samples except that the reactors were wrapped in Al foil. Both dark and light reactors were
163 run in duplicates and they were placed on flat surface at the border of the lake ($66^\circ 17' 04''\text{N}$,
164 $30^\circ 52' 05''\text{E}$). The flasks were exposed to direct unshaded sunlight from July 9 to July 20 during
165 essentially anticyclonic weather. The daytime duration in this period was between 22 and 20.5 hours.
166 The temperature of the experimental reactors followed the diurnal cycle and was equal to $18 \pm 5^\circ\text{C}$
167 over 250 h of exposure, which was within the range of actual water temperature in stream and fen
168 during the month of July^{17,37}. The quartz reactors were sampled after 0, 100 and 200 h of exposure of
169 the fen water (ZPBL) and after 0, 110 and 250 h of exposure of the stream (KAR-1). For each sampling,

170 the whole reactor was sacrificed. The samples were immediately filtered through 0.22 μm Sartorius
171 single-used filter into pre-cleaned polypropylene vials. These waters were then acidified using bi-
172 distilled HNO_3 for trace metals analysis or directly used, without acidification, for DOC, $\text{UV}_{254\text{ nm}}$,
173 DIC and anions determinations. The 0.22 μm filtrate from quartz reactors was additionally ultrafiltered
174 through 1 and 10 kDa regenerated cellulose single-use filters with an Amicon 8400 frontal
175 Ultrafiltration unit (continuously stirred 400-ml polycarbonate cell maintained under 1.5–2 atm
176 pressure). Details of ultrafiltration procedure in humic boreal waters of North Karelia and discussion
177 of possible artifacts are presented elsewhere^{17,37,43}. In these experiments, we consider the behavior of
178 Fe in $<0.22\ \mu\text{m}$ and $<10\ \text{kDa}$ fractions of the stream water and in $<0.22\ \mu\text{m}$, <10 and $<1\ \text{kDa}$ fractions
179 of the fen water.

180 All experiments including controls were run in duplicates (two independent reactors) and both
181 solution duplicates were processed for isotope analyses. Analyses of DOC and Fe concentration in
182 various filtered and ultrafiltered fractions were performed using Shimadzu TOC-VCSN and Agilent
183 ICP MS, following procedures described previously^{27,28}. The DOC was measured with an uncertainty
184 of 3% and a detection limit of $0.1\ \text{mg L}^{-1}$. The total dissolved Fe represents the sum of Fe(II) and
185 Fe(III) in the $<0.22\ \mu\text{m}$ fraction. The uncertainty of Fe concentration measurements ranged from 5 to
186 10% (1SD). The international geostandard SLRS-5 (Riverine Water Reference Material for Trace
187 Metals certified by the National Research Council of Canada) measured each 20 samples was used to
188 check the validity and reproducibility of Fe analysis. Good agreements were found between the
189 replicate measurements of Fe in SLRS-5 and the certified values (relative difference $<20\%$ SD on the
190 repeated measurements).

191 Assessment of Fe(II) and Fe(III) concentrations was performed using the conventional ferrozine
192 method⁴⁵. The efficiency of this method in organic-rich tropical waters was further demonstrated in
193 Rio Negro⁴⁶. Because of possible interferences from DOM in humic boreal waters, the ferrozine
194 method was used employing a standard addition technique. This allowed to achieve a detection limit
195 of $15\ \mu\text{g L}^{-1}$ and an uncertainty from 10-20% at $15 < \text{Fe(II)} < 100\ \mu\text{g L}^{-1}$ to 5-10% at $\text{Fe(II)} > 100\ \mu\text{g}$

196 L⁻¹. Further, we verified the stability of Fe(II) in oxygenated humic waters (pH = 4.6 to 6.5; DOC =
197 20 to 50 mg L⁻¹) using peat and moss leachate (similar to main allochthonous DOM in studied sites⁴⁷).
198 The Fe(II) concentration remained stable within ±10% over 24-180 h of exposure.

199 The Fe(III) and Fe(II) complexation with organic ligands and solution saturation degree with
200 respect to secondary Fe hydroxide in the course of experiment were calculated using Visual
201 MINTEQA⁴⁸, in conjunction with a NICA-Donnan humic ion bonding model, as described previously¹⁷.
202 We considered carboxylic and phenolic complexes of fulvic acids with Fe²⁺ and Fe³⁺ ions, as well as
203 Fe(II) weak (electrostatic) interaction with fulvic acids.

204 For Fe isotope analysis, filtered and acidified water samples were evaporated in the clean
205 laboratory. After acid digestion of the residue using a mixture of HCl and HNO₃, Fe was purified via
206 anion exchange chromatography with HCl using Bio Rad AG1 X4 resin, 200–400 mesh to remove all
207 matrix elements³⁷. For this, we used thermoretractable Teflon columns with an internal diameter of 4
208 mm⁸. The resins were conditioned using 6 M of HCl prior to the sample loading in 0.5 ml of 6 M HCl.
209 The matrix species were eluted in 3 ml of the same acid and, subsequently, Fe was quantitatively eluted
210 with 2 ml of 0.05 M HCl. The purified Fe solutions were evaporated at 120°C. After evaporation,
211 purified Fe samples were redissolved in a 0.05 M HCl solution that was used for the MC-ICP-MS
212 analysis. Iron and the internal standard, Ni, were set to concentration producing signals of ca. 40 V of
213 ⁵⁶Fe and 20V for ⁶⁰Ni. Iron isotope measurements were performed at the CNRS-INSU National MC-
214 ICP-MS facility in Lyon using a Thermo Electron Neptune Plus and at GET-CNRS in Toulouse using
215 a Thermo Electron Neptune MC-ICP-MS (Bremen, Germany)⁴⁹. All analyses are reported in the delta
216 notation relative to the IRMM-014 standard, expressed as δ⁵⁷Fe, which represents the deviation in per
217 mil relative to the reference material:

$$218 \quad \delta^{57}\text{Fe} (\text{‰}) = \left(\frac{(^{57}\text{Fe}/^{54}\text{Fe})_{\text{sample}}}{(^{57}\text{Fe}/^{54}\text{Fe})_{\text{IRMM 14}}} - 1 \right) * 1000$$

219 We also obtained δ⁵⁶Fe values but, since the relationships between δ⁵⁶Fe and δ⁵⁷Fe of the
220 samples plot on a single mass fractionation line (δ⁵⁷Fe = 1.466 × δ⁵⁶Fe + 0.005, R² = 0.9995, p < 10⁻⁶)

221 ⁴), only $\delta^{57}\text{Fe}$ values are discussed in this paper. Data quality was checked by the analysis of our in-
222 house hematite standard every 5 samples in the analytical sequence. Our mean value of $0.771\pm 0.047\%$
223 (2SD) for this standard obtained between Lyon and Toulouse from pooling 51 individual analyses by
224 groups of 6 was consistent with the values of $0.766\pm 0.072\%$ reported previously⁸.

225

226 3. Results and Discussion

227 3.1. Iron in the $< 0.22\ \mu\text{m}$ fraction during biodegradation experiments: Heavier isotopes
228 adsorption onto and lighter isotopes uptake by live cells of *P. aureofaciens*

229 The studied surface waters were oxygenated, organic- and Fe-rich (pH = 7.1, DOC = $12\ \text{mg L}^{-1}$,
230 Fe = $208\ \mu\text{g L}^{-1}$ in KAR-1; pH = 5.4, DOC = $38.7\ \text{mg L}^{-1}$, and Fe = $4310\ \mu\text{g L}^{-1}$ in ZPBL). The
231 stream water contained ~24% of Fe(II) and the fen contained ~20% of Fe(II); the LMW_{<1 kDa} fraction
232 of DOC was sizably higher in the stream compared to the fen (77 and 29%, respectively). The
233 experimental results are reported in Table 1 whereas those of the control experiments are listed in
234 Table S1. The pH value increased by 0.6 and 1.2 unit over 4 days of *P. aureofaciens* reaction with
235 stream water and fen water, respectively (Table 1). There was no sizeable DOC decrease over the first
236 1 h of reaction. The long-term removal (1 – 100 h) of DOC by *P. aureofaciens* was not pronounced in
237 the stream water but was high in the fen water ($-33\pm 5\%$).

238 Iron exhibited initial adsorption after 1 h of reaction as it is seen from the difference between
239 the stream and the fen water control and bacterial suspension at the beginning of experiment (Fig. 2 A
240 and B and Table 1). The proportions of fast adsorption (0-1 h) and assimilation/coagulation (1-93 h)
241 relative to total Fe removal in the experiments were respectively equal to 35% and 37% in the stream
242 water and 30% and 25% in the fen water. In the latter, the concentration of divalent Fe decreased
243 almost 3-fold over the first day of reaction relative to control (Fig. 2 C). No sizeable change of Fe(II)
244 in stream water could be assessed because the Fe(II) concentration in KAR-1 (not shown) was 30 ± 20
245 $\mu\text{g/L}$ (~16% of total dissolved Fe), with a quantification limit of Fe(II) by this method of $15\ \mu\text{g/L}$ ⁴⁵.

246 All initial solutions were undersaturated with respect to Fe-bearing minerals. Calculated
247 change of Fe(II) and Fe(III) speciation in the course of experiments demonstrated the dominance of
248 Fe(III)-fulvic acid (FA) complexes. The Fe(II) bound to FA fully disappeared in the stream and
249 decreased by a factor of 3 in the fen waters (**Fig. S1**). Specifically, the Fe(III) complex with carboxylic
250 groups of FA degraded 4-fold in both fen and stream water, whereas phenolic complex of Fe(III)
251 remained stable (**Table S2**). The proportion of Fe(II) complex with carboxylates of FA increased
252 whereas Fe(II)-weak electrostatic complex completely disappeared. This is consistent with highly
253 reactive behavior of dissolved Fe(II) in biodegradation experiments.

254 The second $< 0.22 \mu\text{m}$ filtration step in the laboratory of the control water samples showed that
255 the 6 months storage in the fridge did not affect stream water chemical composition but it induced a
256 decrease of Fe concentration in the fen water from $4310 \mu\text{g/L}$ to $2470 \mu\text{g/L}$, accompanied by a change
257 in $\delta^{57}\text{Fe}$ from $0.25 \pm 0.06\text{‰}$ to $1.06 \pm 0.04\text{‰}$. A strong $\delta^{57}\text{Fe}$ increase from $1.59 \pm 0.05\text{‰}$ to $2.87 \pm 0.07\text{‰}$
258 also resulted from the storage for the stream water (Table 1 and S1). This change could be linked to
259 some $\text{Fe}(\text{OH})_3$ precipitation due to either coagulation of Fe(III)-rich organic colloids or Fe(II)
260 oxidation. To preserve at least the Fe isotopic composition of DOC-rich waters over several months,
261 immediate freezing after filtration in the field on the sampling site is preferable⁵⁰, but this is not always
262 possible for logistical reasons.

263 Although the fractionation of Fe between bacterial cells and organo-ferric colloids has not been
264 studied previously, the adsorption of metal cations such as Zn^{2+} at the microorganism cell surface is
265 known to favor the heavier isotopes⁵¹ and both Fe^{2+} and Fe^{3+} ions follow this rule^{30,31}. The heavier Fe
266 isotopes are preferentially adsorbed onto solid surfaces during equilibrium isotope fractionation
267 processes³⁶. Experiments that lasted 11 days with anaerobic phototrophic Fe-oxidizing, aerobic
268 neutrophilic Fe-oxidizing, and heterotrophic Fe-reducing bacteria demonstrated that metabolically-
269 produced hydrous ferric oxide (HFO) exhibited heavier isotopic composition than the initial Fe(II),
270 with a fractionation factor ($\Delta^{57}\text{Fe}$) of $+2.2 \pm 0.3\text{‰}$ ⁵². Further, depending on the phytoplankton species
271 and the composition of the culture medium, the cell surface was found to be enriched in heavier

272 isotopes by $+2.4 \pm 0.6$ ‰ to $+2.9 \pm 0.1$ ‰ for Fe^{2+} containing solution and by $+0.4 \pm 0.2$ to $+1.0 \pm 0.2$ ‰
273 for Fe^{3+} solution³⁰. More recent measurements of Fe isotope fractionation during Fe adsorption onto
274 phytoplankton cells quantitatively confirmed these data³¹. The value $\Delta^{57}\text{Fe}_{\text{cell-solution}}$ of $+0.5 \pm 0.1$ ‰ for
275 the river water inferred from the present study suggests essentially Fe^{3+} ion adsorption onto *P.*
276 *aurefaciens* cell surfaces, presumably forming Fe(III)-phosphoryl complexes⁴⁴. Note however that the
277 competition between surface organic moieties and aqueous organic complexes for heavy Fe isotopes
278 can decrease the magnitude of isotopic offset in humic waters compared to experimental solutions with
279 low DOC. At present, the isotopic offset for adsorption of organo-ferric colloids onto organic surfaces
280 is not known and this should be the subject of future research.

281 The interaction of stream water with heterotrophic bacterium produced first, a drop in $\delta^{57}\text{Fe}$ of
282 ca 0.4‰ in solution due to adsorption of heavier isotopes on the cell surface, and then a gradual
283 increase in aqueous $\delta^{57}\text{Fe}$ from $+2.5 \pm 0.1$ ‰ to $+3.2 \pm 0.1$ ‰ between 1 and 24 h (Fig. 3 A) yielding
284 $\Delta^{57}\text{Fe}_{\text{cell-solution}}$ of -0.7‰. This implies removal of lighter Fe isotopes due to their preferential
285 intracellular uptake. After an initial drop in the stream water $\delta^{57}\text{Fe}$, the long-term removal of lighter
286 Fe isotopes by live bacteria produced ca 0.7‰ increase in $\delta^{57}\text{Fe}$ over the first 20 h of reaction that
287 remained constant to 50 h (Fig. 3A). This strongly supports biological mechanism of lighter Fe
288 isotopes uptake inside cells rather than metabolically-induced $\text{Fe}(\text{OH})_3$ precipitation. In the latter case,
289 the solid phase would be enriched in heavy isotope ($\Delta^{57}\text{Fe}_{\text{FeOOH-Fe(aq)}} = +1.5$ to $+4-5$ ‰)^{32,53,54} as also
290 supported by natural observations^{9,53}. The present result is at variance with previous Fe assimilation
291 by magnetotactic bacteria³³ or phytoplankton⁴² that inferred a heavier Fe isotope uptake inside the cells
292 due to a combined Fe oxidation. However, the Fe(III)-DOM complexes in solution retain heavy isotope
293 as it is known for $\text{Fe}^{3+}(\text{H}_2\text{O})_6$ -Fe(III) chelate (DFO-B): the organic complexes are enriched in heavy
294 isotopes with an isotopic offset of $+0.90 \pm 0.23$ ‰⁵⁵, and overall, there is a strong positive correlation
295 between Fe fractionation factors and the Fe-binding affinity of the ligands⁵⁶. According to vMinteq
296 calculation, the majority of Fe in our experimental solutions was bound to phenolic complexes with

297 fulvic acids (Fig. S1, Table S2). Therefore, we suggest that strong complexation of isotopically heavy
298 Fe(III) with DOM prevents the intracellular uptake of heavier Fe isotopes.

299 In the fen water, we observed a similar $\delta^{57}\text{Fe}$ evolution during biodegradation experiments,
300 though with smaller variations. The isotopic composition of dissolved Fe did not appreciably change
301 during *P. aureofaciens* short-term interaction with fen water: we observed only weak adsorption of
302 heavy isotope ($<0.1\text{‰}$) and a weak assimilation of light isotopes $\Delta^{57}\text{Fe}_{\text{cell-solution}} \leq 0.1\text{‰}$ over first 40
303 h (Fig. 3 B). Relative to the sterile control, a decrease in $\delta^{57}\text{Fe}$ at the beginning of experiment signified
304 preferential adsorption of heavy isotopes with $\Delta^{57}\text{Fe}_{\text{cell-solution}} = +0.2 \pm 0.1\text{‰}$. Over 100 h of reaction,
305 light Fe isotopes were taken up by the cells as the $\delta^{57}\text{Fe}$ of solution increased from $+0.86 \pm 0.1\text{‰}$ to
306 $+1.05 \pm 0.05\text{‰}$.

307 Overall, the effect of bio-transformation of Fe isotopic signature were much stronger in the stream
308 water compared to the fen water, which may be due to different concentration of Fe in these two
309 samples (200 and 4300 $\mu\text{g/L}$) at otherwise similar bacterial concentration (1 $\text{g}_{\text{wet}}/\text{L}$). As a result, there
310 was an order of magnitude higher ligand : metal ratio ((cell surface sites) : Fe fraction) in the stream
311 compared to the fen water.

312

313 *3.2. Iron concentrations and isotopic signatures evolution during photodegradation of organo-ferric*
314 *colloids: Removal of heavier isotopes due to Fe(III) hydroxide formation and appearance of*
315 *isotopically light Fe(II) in the LMW fraction*

316 There was no pH variation in the course of photodegradation experiments: within the uncertainty
317 of duplicates ($< 0.1\text{-}0.2$ pH unit), the pH in the dark control and the light experiment was identical and
318 equal to 7.0 ± 0.2 and 5.3 ± 0.1 in the stream and fen water, respectively (Table 1 and S1). The DOC
319 concentration in $<0.22 \mu\text{m}$ fraction of stream and fen water decreased by 30 and 50%, respectively,
320 over 200 to 250 h of photodegradation experiment (Table 1). There was a good correlation between
321 ultraviolet absorbency ($\text{UV}_{254 \text{ nm}}$) and Fe concentration in the fen water ($R^2 = 0.928$) which was absent
322 in the stream water in the course of experiment ($R^2 = 0.19$).

323 In the stream water, Fe concentration remained generally constant within the uncertainties over
324 250 h of exposure to sunlight, relative to the dark control, and no formation of flocculent material was
325 noted (Fig. 4 A). There was 50 to 80% removal of Fe(II), between 110 and 250 h of exposure, which
326 occurred for both $<0.22 \mu\text{m}$ and $<10 \text{ kDa}$ fractions (from 50 to 15 $\mu\text{g/L}$ and from 20 $\mu\text{g/L}$ to $<$ limit of
327 quantification, respectively, Fig. 4 B).

328 The removal of Fe during fen water exposure to sunlight was strong in the $\leq 0.22 \mu\text{m}$ fraction
329 ($\sim -75\%$ of initial concentration) and did not occur in the $\leq 10 \text{ kDa}$ fraction ($\leq 7\%$ of the initial
330 concentration, Fig. 4 D and Table 1). A notable increase in total Fe concentration (ca. 210%) in the
331 $\text{LMW}_{<1 \text{ kDa}}$ fraction was observed over 200 h of exposure (Fig. 4 D). The divalent Fe concentration
332 decreased by 50% in the $\leq 0.22 \mu\text{m}$ fraction but strongly increased ($\sim 500\%$) in the $\leq 1 \text{ kDa}$ fraction
333 (Fig. 4 E and Table 1). Over 196 h of irradiation, the Fe(II) proportion increased from 20 to 50% in
334 the $\leq 0.22 \mu\text{m}$ fraction and from 35 to 55% in the $< 1 \text{ kDa}$ fraction. The $\leq 10 \text{ kDa}$ fraction did not
335 demonstrate any difference in Fe(II) concentration between the sunlight-irradiated samples and the
336 dark control.

337 During sunlight exposure, the $\leq 0.22 \mu\text{m}$ fraction of the fen water became depleted in Fe as the
338 molar ratio of $C_{\text{org}}:\text{Fe}$ increased from 50 to 100. This trend mainly stems from more efficient Fe
339 removal compared to DOC (Table 1). The change of this ratio in the stream water was within the
340 experimental uncertainty. The $C_{\text{org}}:\text{Fe}$ ratio in the fen water colloids ($1 \text{ kDa} - 0.22 \mu\text{m}$) did not change
341 in the course of photo-degradation, from 31 at the beginning of experiment to 32 after 193 h of sunlight
342 exposure. In the $\text{LMW}_{<1 \text{ kDa}}$ fraction of fen water, the $C_{\text{org}}:\text{Fe}$ ratio decreased from 247 to 126.

343 All size fractions of the initial stream solution and the $\text{LMW}_{<1 \text{ kDa}}$ fraction of the fen water were
344 undersaturated with respect to Fe-bearing minerals. The initial $< 0.22 \mu\text{m}$ fen water was supersaturated
345 with respect to goethite, lepidocrocite and magnetite (Saturation Indexes = 1.3, 0.62, and 3.6,
346 respectively). The speciation calculation using vMinteq also demonstrated that Fe(III) is fully
347 complexed with DOM (Fig. S2). Therefore, the removal of Fe in the form of particulate Fe hydroxide
348 could be only due to liberation of part of Fe from organic complexes after photolytic degradation of

349 colloidal DOM that stabilized Fe (III) polymers in solutions. Calculated Fe(II) and Fe(III) speciation
350 in the fen water before and after photodegradation experiment demonstrated an appearance of ~2% of
351 inorganic Fe(II) and approx. 2-fold increase of Fe(II) bound to DOM, in both < 0.22 μm and < 1 kDa
352 size fraction (**Fig. S2**). In the stream water, there was a 3-fold decrease of Fe(II) bound to DOM.
353 Specifically, the Fe(III) complex with carboxylic groups of FA decreased and increased 3-fold in fen
354 and stream waters, respectively (**Table S3**). Phenolic complexes of Fe(III) which accounted for
355 >93...99% of all Fe, remained constant in the course of experiment. In the fen water, the proportion
356 of Fe(II)-weak electrostatic complex strongly decreased (by a factor of 4.5 and 1.5 in < 0.22 μm and
357 < 1 kDa fractions, respectively) whereas Fe(II) complex with FA carboxylates increased in < 0.22 μm
358 fraction and stayed constant in < 1 kDa fraction (**Table S3**). According to vMinteq predictions, 4.5×10^{-5}
359 M of ferrihydrite should could have precipitated from the fen water over 200 h of solar irradiation.
360 This is equivalent to ~2250 $\mu\text{g/L}$ of dissolved Fe concentration decrease, which is comparable to the
361 range encountered in the experiment (ca. 3400 $\mu\text{g/L}$, see **Fig. 4 D** and **Table 1**).

362 The isotopic signature of stream water samples remained constant in the < 0.22 μm fraction of
363 dark control and sun-light irradiated quartz reactors (**Fig. 5A**). The $\delta^{57}\text{Fe}$ value of the < 10 kDa fraction
364 decreased from $+2.93 \pm 0.05\text{‰}$ to $+1.92 \pm 0.1\text{‰}$ after first 110 h of exposure and then remained constant.
365 Note that the initial < 10 kDa fraction of stream water was ca. 1.5 ‰ isotopically heavier than the <
366 0.22 μm fraction, in agreement with previous measurement of Fe isotopic composition in colloids of
367 Northern Karelian streams³⁷.

368 The isotopic ratio in the dark control of fen water remained stable at $\delta^{57}\text{Fe} = 0.2 \pm 0.3\text{‰}$, except
369 in the LMW< 1 kDa fraction, where a $+0.6\text{‰}$ increase was observed, related to to the Fe and DOC loss
370 (**Table S1**). Similar effect was reported in the organic-rich Negro River where it was attributed to the
371 loss of isotopically light «heteroaggregates»⁵⁰. In contrast to dark controls, sunlight irradiation of the
372 fen water strongly impacted $\delta^{57}\text{Fe}$ in all 3 fractions, <0.22 μm , <10 kDa and <1 kDa (**Fig. 5 B**). Over
373 first 100 h of reaction, there was sizeable, from 1 to 2‰, decrease of $\delta^{57}\text{Fe}$ in the <0.22 μm and the

374 <1-10 kDa fraction, respectively. Over the next 100 h, the $\delta^{57}\text{Fe}$ further decreased by 1.5 ‰ in the
375 <0.22 μm fraction and stabilized at $\delta^{57}\text{Fe} = -2.2 \pm 0.2\text{‰}$ in the <1 and <10 kDa fractions.

376 Sunlight exposure of stream water did not produce any sizable change of Fe concentration and
377 isotopic signature in the < 0.22 μm fraction (**Fig. 4A** and **5A**), in general agreement with stability of
378 boreal high latitude metal concentration in riverwaters with respect to sunlight irradiation^{28,57}. After
379 100 h of sunlight irradiation, the < 10 kDa fraction of stream water became 1.5‰ lighter compared to
380 the initial value or the dark control (**Fig. 5A**). A plausible explanation for this isotopic pattern invokes
381 the presence of strong low molecular weight (< 10 kDa) Fe(III)-organic ligand (chelate) complexes
382 which are enriched in heavy isotopes⁵⁵. For example, aquatic prokaryotes produce the LMW (0.3 – 1
383 kDa) Fe(III) siderophores⁵⁸. These light sensitive, presumably aromatic Fe complexes represent a
384 small iron fraction of overall $\text{Fe}_{<10 \text{ kDa}}$ pool, but our results indicate that it exhibits a very high $\delta^{57}\text{Fe}$
385 value. The isotopic signature of LMW_{<1-10 kDa} Fe poor, C-rich fraction of Karelian waters reaches
386 +4.2‰³⁷. We hypothesize that these isotopically heavy Fe-organic complexes have low residence time
387 in the river channel and are produced due to periphyton or plankton metabolic activity.

388 The Fe in the fen water was strongly sensitive to sunlight irradiation as > 70% Fe was removed
389 from the <0.22 μm fraction and all filtrates and ultrafiltrates became strongly impoverished in heavy
390 isotopes (**Fig. 4 D, 5 B**). The removal of Fe followed that of SUVA_{254} decrease²⁸, suggesting that the
391 majority of Fe that is removed from the fen water was bound to aromatic (colored) organic carbon.
392 This is also confirmed by the dominance of Fe(III)-phenolic groups of FA in Fe speciation (**Table S3**).
393 It is possible that the photolysis of Fe-DOM complexes liberates ionic Fe which could be removed
394 from solution in the form of isotopically heavy Fe hydroxides. The removal of heavy isotopes by
395 sunlight oxidation of organo-ferric colloids observed in this study (+2.3 \pm 0.1‰) is generally consistent
396 with known fractionation of Fe between Fe(III) hydroxide and Fe(II) solution: ($\Delta^{57}\text{Fe}_{\text{FeOOH-Fe(aq)}} =$
397 +2.3 \pm 0.3‰, ref. 52-54).

398 In contrast to what was hypothesized in our earlier work on these waters³⁷, no enrichment in heavy
399 isotopes of LMW fraction was observed during photolysis of humic waters. Here we suggest that Fe(II)

400 generated in the < 1 kDa fraction is enriched in light isotopes compared with initial Fe(III) in colloids,
401 thus producing overall negative $\delta^{57}\text{Fe}$ value in $\text{LMW}_{<1\text{ kDa}}$ after irradiation. Assuming an equilibrium
402 fractionation factor between Fe(II) and Fe(III) of -4.3‰ ⁵⁹ and considering the starting water $\delta^{57}\text{Fe}$
403 close to 0‰ (Fig. 5B), the 55% of Fe(II) in < 1 kDa fraction (Fig. 4F) provides $0.55 \times (-4.3\text{‰}) = -$
404 2.4‰ of $\delta^{57}\text{Fe}$, in full agreement with values shown in Fig. 5B. This $< 0.22\ \mu\text{m}$ fraction comprises two
405 Fe pools: (1) Fe remaining after $\text{Fe}^{2+}(\text{aq}) \rightarrow \text{Fe}(\text{OH})_3$ and after $\text{Fe}^{3+}(\text{colloidal}) \rightarrow \text{Fe}(\text{OH})_3$
406 precipitation, and (2) isotopically light Fe^{2+} produced in the LMW fraction. It is important to note that
407 the photolysis of organo-ferric colloids which represents 80% of Fe in $< 0.22\ \mu\text{m}$ fraction, removes
408 Fe(III) in the form of $\text{Fe}(\text{OH})_3$ hydroxides corresponding to $\Delta^{57}\text{Fe}_{\text{Fe(III)hydroxide-Fe(aq)}}$ of $2.4 \pm 0.1\text{‰}$, Fig
409 5B. The observed enrichment of solid phase in heavier isotopes is therefore similar to $\text{Fe}^{2+}(\text{aq}) \rightarrow$
410 $\text{Fe}(\text{OH})_3$ reaction ($\Delta^{57}\text{Fe}_{\text{Fe(III)hydroxide-Fe(aq)}} = 2.4\ \text{‰}$ ⁵²) rather than to $\text{Fe}^{3+}(\text{aq}) \rightarrow \text{Fe}(\text{OH})_3$ reaction
411 ($\Delta^{57}\text{Fe}_{\text{Fe(III)hydroxide-Fe(aq)}} = -0.9\ \text{‰}$ ⁶⁰). Note here that in the photolysis experiments, the loss of dissolved
412 Fe and change of Fe isotope fractionation are mainly interpreted as precipitation of hydrous Fe(III)-
413 oxides. We therefore neglect Fe(II) sorption onto hydrous Fe(III)-oxides and subsequent atom
414 (isotope) exchange between Fe(II) and hydrous Fe(III)-oxides. These processes are responsible for
415 substantial Fe isotope fractionation in a number of organic-free systems^{36, 61-64}. In humic waters, both
416 remaining $\text{Fe(II)}_{\text{aq}}$ ions and $>\text{FeOOH}$ surface sites of newly precipitated Fe(III) hydroxides are likely
417 to be bound to carboxylic and phenolic groups of fulvic acids. These surface organic - Fe complexes
418 interfere with Fe(II)-Fe(III) hydroxide isotope exchange which would therefore require special
419 investigation. Further, in order to fully account for short-term variation of Fe concentration, speciation
420 and isotope ratios, one has to consider both dissolved and particulate Fe fractions, as well as isotopic
421 composition of both Fe(II) and Fe(III) species.

422 We observed quite large differences in the degree of Fe concentrations and Fe isotopic
423 composition during photolysis of the fen and the stream water. These differences may stem from the
424 combination of two main factors controlling the degree of DOM and Fe photo-reactivity in natural
425 waters: the fen water is a 1.5 unit of pH lower than the stream and has a factor of 30 higher in Fe

426 concentration. The water acidity is known to exert a strong positive effect on the photolysis of
427 DOM^{65,66} and the DOM photobleaching is enhanced by elevated Fe concentration via the photo-Fenton
428 effect below pH 6⁶⁷. Overall, in natural settings, one may expect large variation of Fe and DOM photo-
429 liability depending on the environmental context. Thus, slightly alkaline (pH = 8) surface water from
430 a temperate peatland in China exhibited quite higher photo-stability of Fe⁶⁸, whereas acidic DOC-rich
431 waters from a subtropical swamp under UV irradiation demonstrated 10 times more efficient removal
432 of Fe relative to DOC⁶⁹. As such, depending on the lithological context of peatlands (i.e., acidic (felsic)
433 or carbonate (sedimentary) rocks), the degree of Fe chemical and isotopic composition change under
434 sunlight may be dramatically different.

435

436 3.3. Complexity of Fe isotope fractionation in boreal humic waters and implication for inland 437 waters Fe isotope budget

438 We hypothesize several processes responsible for chemical removal and isotopic redistribution of
439 Fe among different colloidal pools in DOM- and Fe-rich stream and fen water, shown schematically
440 in Fig. 6. High molecular size (10 kDa – 0.45 μm) organo-ferric colloids representing the majority of
441 dissolved (<0.22 μm) Fe^{17,37} are stabilized by organic ligands originating from topsoil and bog peat
442 leaching. In addition, a small fraction of Fe(III) could be linked to highly specific, LMW_{<1-10 kDa} ligands
443 having a short residence time in the river channel; these complexes could be produced via in-stream
444 plankton and periphyton activity. In the fen water, a sizeable fraction of Fe is in the form of Fe(II)
445 inorganic and organic complexes⁷⁰. In the river water, the HMW colloids are subjected to biologically-
446 controlled transformations via *i*) adsorption onto surfaces of aquatic bacteria, favoring heavier isotopes
447 to the cells, with an overall $\Delta^{57}\text{Fe}_{\text{cell ads-solution}} = +0.4 \pm 0.1\%$, and *ii*) assimilation by live bacteria,
448 favoring lighter Fe isotopes to the cells with $\Delta^{57}\text{Fe}_{\text{cell incorp-solution}} = -0.7 \pm 0.1\%$. On a short-term scale
449 (hours), the humic waters, once placed in contact with bacteria, are therefore becoming enriched in
450 lighter Fe isotopes, followed, on a long-term scale (days), by enrichment in heavier Fe isotopes.
451 Considering available data on preferential heavy isotope adsorption onto phytoplanktonic and

452 peryphytic cyanobacteria inhabiting natural waters (from +0.4 to +2.9‰, ref. 30), and neglecting
453 Rayleigh distillation processes given that we are dealing with open systems (hydrological continuum,
454 ref. 17), the overall magnitude of diurnal variation of dissolved (< 0.45 μm) δ⁵⁷Fe in small streams and
455 stagnant surface waters in the presence of common soil bacteria may range from +2.7‰ to +0.7‰.
456 This greatly exceeds the range of Fe isotopic excursions in various sediments and in all possible
457 bedrocks⁷¹.

458 Further, photolysis of DOM and Fe-DOM complexes in surface waters, which operates at the
459 time scale comparable to water and solute residence time in these waters (1-10 days), is capable to
460 dramatically enrich in lighter Fe isotopes (by 1.5 to 2.5‰) of both dissolved (<0.22 μm) and LMW<1-
461 10 kDa water fraction. We suggest that the two major processes of organo-ferric colloid transformation
462 under sunlight in natural waters include: (i) degradation of the organic part of colloids (1 kDa – 0.22
463 μm) and production of low molecular weight (< 1 kDa) organic ligands including carboxylic and
464 aromatic chelates capable of strong binding of Fe ions; (ii) coagulation and precipitation of Fe-rich
465 oxy(hydroxide) after the solar radiation-induced removal of stabilizing organic matter.

466 The enigmatic enrichment of the LMW fraction (<1-10 kDa) of the stream water in heavy
467 isotopes³⁷ is therefore most likely linked to strong, presumably aromatic, isotopically heavy Fe(III)-
468 organic complexes. These compounds have low residence time and are produced in the river channel
469 due to periphyton or plankton metabolic activity. In addition, sunlight irradiation of subarctic humic
470 waters may produce 10-fold increase in aliphatic and aromatic carbonic acids⁷² capable to bind both
471 Fe(II) and Fe(III). Altogether, bio- and photo-degradation of dissolved Fe in river, stream and bog
472 waters can produce from -2 to +3 ‰ δ⁵⁷Fe variation on time scales of a few days. Because this time
473 is generally shorter than the water residence time in surface waters, considering of Fe isotopic signature
474 of rivers and streams as a conservative value inherited from soils and using it for tracing the sources
475 and weathering regime on watersheds are not warranted at short time- and length-scales. Therefore,
476 naturally-induced variations in biological activity (switching from heterogenic bacteria uptake to
477 adsorption onto aquatic phototrophs) and sunlight illumination can modify the overall Fe isotopic

478 signatures of surface waters by several permil. Moreover, when considering the processes responsible
479 for Fe chemical and isotopic transformation in organic-rich streams, one has to assess both dissolved
480 (<0.45 or <0.22 μm) and LMW_{< 1-10 kDa} fractions of metal, since their isotopic signatures and photo-
481 susceptibility may be dramatically (by 1 to 3‰) different.

482

483 **Acknowledgements**

484

485 We acknowledge support from a RFBR research project № 17-05-00342_a, and the CNRS (PRC) No
486 1070 project. We thank P. Télouk in Lyon and J. Chmeleff in Toulouse for maintaining the MC-ICP-
487 MS instruments in good working order, and M. Henri for maintaining the clean room in Toulouse.

488

489 **References**

- 490 (1) Beard, B.L.; Johnson, C.M.; Von Damm, K.L.; Poulson, R.L. Iron isotope constraints on Fe
491 cycling and mass balance in oxygenated Earth oceans. *Geology* **2003**, *31*, 629-632.
- 492 (2) Labatut, M.; Lacan, F.; Pradoux, C.; Chmeleff, J.; Radic, A.; Murray, J.W.; Poitrasson, F.;
493 Johansen, A.M.; Thil, F. Iron sources and dissolved-particulate interactions in the seawater of the
494 Western Equatorial Pacific, iron isotope perspectives. *Global Biogeochem. Cycles* **2014**, *28*, 1044-
495 1065.
- 496 (3) Ingri, J.; Malinovsky, D.; Rodushkin, I.; Baxter, D.C.; Widerlund, A.; Andersson, P.;
497 Gustafsson, O.; Forsling, W.; Ohlander, B. Iron isotope fractionation in river colloidal matter. *Earth*
498 *Planet. Sci. Lett.* **2006**, *245* (3-4), 792-798.
- 499 (4) Ingri, J.; Conrad, S.; Lidman, F.; Nordblad, F.; Engstrom, E.; Rodushkin, I.; Porcelli, D. Iron
500 isotope pathways in the boreal landscape: Role of the riparian zone. *Geochim. Cosmochim. Acta* **2018**,
501 *239*, 49-60.
- 502 (5) Escoube, R.; Rouxel, O.; Pokrovsky, O.S.; Schroth, A.; Holmes, R.M.; Donard, O.F.X. Iron
503 isotope systematics in Arctic rivers. *Comptes Rendus Geoscience* **2015**, *347* (7-8), 377-385; DOI
504 10.1016/j.crte.2015.04.005.
- 505 (6) Conrad, S.; Ingri, J.; Gelting, J.; Nordblad, F.; Engström, E.; Rodushkin, I.; Andersson, P.S.;
506 Porcelli, D.; Gustafsson, Ö.; Semiletov, I.; Öhlander, B. Distribution of Fe isotopes in particles and
507 colloids in the salinity gradient along the Lena River plume, Laptev Sea. *Biogeosciences*, **2019**, *16*,
508 1305-1319, <https://doi.org/10.5194/bg-16-1305-2019>.
- 509 (7) Chen, J.B.; Busigny, V.; Gaillardet, J.; Louvat, P.; Wang, Y.N. Iron isotopes in the Seine River
510 (France): Natural versus anthropogenic sources. *Geochim. Cosmochim. Acta* **2014**, *128*, 128-143.
- 511 (8) Poitrasson, F.; Vieira, L.C.; Seyler, P.; dos Santos Pinheiro, G.M.; Mulholland, D.S.; Bonnet,
512 M.P.; Martinez, J.M.; Lima, B.A.; Allard, T.; Boaventura, G.R.; Chmeleff, J.; Dantas, E.; Guyot, J.L.;
513 Mancini, L.; Pimentel, M.M.; Santos, R.V.; Sondag, F.; Vauchel, P. Iron isotope composition of the
514 bulk waters and sediments from the Amazon River Basin. *Chem. Geol.* **2014**, *377*, 1-11.
- 515 (9) Song, L.; Liu, C.-Q.; Wang, Z.-L.; Zhu X.; Teng, Y.; Liang, L.; Tang, S.; Li, J. Iron isotope
516 fractionation during biogeochemical cycle: information from suspended particulate matter (SPM) in
517 Aha Lake and its tributaries, Guizhou, China. *Chem. Geol.* **2011**, *280* (1-2), 170-179.
- 518 (10) Busigny, V.; Planavsky, N.J.; Jezequel, D.; Crowe, S.; Louvat, P.; Moureau, J.; Viollier, E.;
519 Lyons, T.W. Iron isotopes in an Archean ocean analogue. *Geochim. Cosmochim. Acta* **2014**, *133*, 443-
520 462.

- 521 (11) Serikova, S.; Pokrovsky, O.S.; Ala-aho, P.; Kazantsev, V.; Kirpotin, S.; Kopysov, S.; Krickov,
522 I.; Laudon, H.; Manasypov, R.M.; Shirokova, L.S.; Soulsby, C.; Tetzlaff, D.; Karlsson, J. High riverine
523 CO₂ emissions at the permafrost boundary of Western Siberia. *Nature Geoscience* **2018**, *11*, 825-829.
- 524 (12) Serikova, S., Pokrovsky, O.S., Laudon, H., Krickov, I.V., Lim, A.G., Manasypov, R.M.,
525 Karlsson, J. High carbon emissions from thermokarst lakes of Western Siberia. *Nature Comm.*, **2019**,
526 *10*, Art No 1552. <https://doi.org/10.1038/s41467-019-09592-1>.
- 527 (13) Kritzberg, E.S.; Villanueva, A.B.; Jung, M.; Reader, H.E. Importance of boreal rivers in
528 providing iron to marine waters. *PLoS ONE* **2014**, *9*, e107500, DOI 10.1371/journal.pone.0107500.
- 529 (14) Hirst, C.; Kutscher, L.; Murphy, M.; Shaw, S.; Burke, I.T.; Kaulich, B.; Maximov, T.;
530 Pokrovsky, O.S.; Mörh, C.-M.; Andersson, P.S.; Porcelli, D. Characterization and stability of Fe-
531 bearing particles in the Lena River catchment, NE Russia. *Geochim. Cosmochim. Acta* **2017**, *213*, 553–
532 573.
- 533 (15) Hasselov, M.; Von Der Kammer, F. Iron oxides as geochemical nanovectors for metal
534 transport in soil–river systems. *Elements* **2008**, *4* (6), 401–406.
- 535 (16) Vonk, J.E.; Tank, S.E.; Bowden, W.B.; Laurion, I.; Vincent, W.F.; Alekseychik, P.; Amyot,
536 M.; Billet, M.F.; Canário, J.; Cory, R.M.; Deshpande, B.N.; Helbig, M.; Jammet, M.; Karlsson, J.;
537 Larouche, J.; MacMillan, G.; Rautio, M.; Walter Anthony, K.M.; Wickland, K.P. Reviews and
538 Syntheses: Effects of permafrost thaw on Arctic aquatic ecosystems. *Biogeosciences* **2015**, *12*, 7129-
539 7167.
- 540 (17) Ilina, S.M.; Lapitsky, S.A.; Alekhin, Y.V.; Viers, J.; Benedetti, M.; Pokrovsky, O.S.
541 Speciation, size fractionation and transport of trace element in the continuum soil water – mire – lake
542 – river – large oligotrophic lake of a subarctic watershed. *Aquat. Geochem.* **2016**, *22* (1), 65-95.
- 543 (18) Shirokova, L.S.; Bredoire, R.; Rolls, J.-L.; Pokrovsky, O.S. Moss and peat leachate
544 degradability by heterotrophic bacteria: fate of organic carbon and trace metals. *Geomicrobiology J.*
545 **2017**, *34* (8), 641-655.
- 546 (19) Kopacek, J.; Klementova, S.; Norton, S.A. Photochemical production of ionic and particulate
547 aluminum and iron in lakes. *Environ. Sci. Technol.* **2005**, *39*, 3656–3662.
- 548 (20) Shiller, A.M.; Duan, S.; van Erp, P.; Bianchi, T.S. Photo-oxidation of dissolved organic
549 matter in river water and its effect on trace element speciation. *Limnol. Oceanography* **2006**, *51*(4),
550 1716–1728
- 551 (21) Mann, P.J.; Sobczak, W.V.; LaRue, M.M.; Bulygina, E.; Davydova, A.; Vonk, J.E.; Schade,
552 J.; Davydov, S.; Zimov, N.; Holmes, R.M.; Spencer, R.G.M. Evidence for key enzymatic controls on
553 metabolism of Arctic river organic matter. *Global Change Biol.* **2014**, *20* (4), 1089-1100.
- 554 (22) Vähätalo, A.V.; Salonen, K.; Münster, U.; Järvinen, M.; Wetzel, R.G. Photochemical
555 transformation of allochthonous organic matter provides bioavailable nutrients in a humic lake. *Acta*
556 *Hydrobiol.* **2003**, *156*, 287-314.
- 557 (23) Kelton, N.; Molot, L.A.; Dillon, P.J. Effect of ultraviolet and visible radiation on iron lability
558 in boreal and artificial waters. *Aquat. Sci.* **2007**, *69*, 86–95.
- 559 (24) Garg, S.; Ito, H.; Rose, A.L.; Waite, T.D. Mechanism and kinetics of dark iron redox
560 transformations in acidic natural organic matter solutions. *Environ. Sci. Technol.* **2013**, *47*, 1861-1867.
- 561 (25) Blazevic, A.; Orłowska, E.; Kandioller, W.; Jirsa, F.; Keppler, B.K.; Tafili-Krueziu, M.;
562 Linert, W.; Krachler, R.F.; Krachler, R.; Rompel, A. Photoreduction of terrigenous Fe-humic
563 substances leads to bioavailable iron in oceans. *Angew. Chem. Int. Ed.* **2016**, *55*, 6417-6422.
- 564 (26) Oleinikova, O.V.; Shirokova, L.S.; Drozdova, O.Yu.; Lapitskiy, S.A.; Pokrovsky, O.S. Low
565 biodegradability of dissolved organic matter and trace metals from subarctic waters. *Sci. Total Env.*
566 **2018**, *618*, 174-187.
- 567 (27) Oleinikova, O.V.; Shirokova, L.S.; Gérard, E.; Drozdova, O.Yu.; Lapitskiy, S.A.; Bychkov, A.Yu;
568 Pokrovsky, O.S. Transformation of organo-ferric peat colloids by a heterotrophic bacterium. *Geochim.*
569 *Cosmochim. Acta* **2017**, *205*, 313-330.
- 570 (28) Oleinikova, O.V.; Drozdova, O.Yu.; Lapitskiy, S.A.; Demin, V.V.; Bychkov, A.Yu;
571 Pokrovsky, O.S. Dissolved organic matter degradation by sunlight coagulates organo-mineral colloids

572 and produces low-molecular weight fraction of metals in boreal humic waters. *Geochim. Cosmochim.*
573 *Acta* **2017**, *211*, 97-114.

574 (29) Beard, B.L.; Johnson, C.M.; Cox, L.; Sun, H.; Nealsen, K.H.; Aguilar, C. Iron isotope
575 biosignatures. *Science* **1999**, *285* (5435), 1889-1892.

576 (30) Mulholland, D.S.; Poitrasson, F.; Shirokova, L.S.; Gonzalez, A.; Pokrovsky, O.S.;
577 Boaventura, G.R.; Vieira, L.C. Iron isotope fractionation during Fe(II) and Fe(III) adsorption on
578 cyanobacteria. *Chem. Geol.* **2015**, *400*, 24-33.

579 (31) Swanner, E.D.; Bayer, T.; Wu, W.; Hao, L.; Obst, M.; Sundman, A.; Byrne, J.M.; Michel, F.M.;
580 Kleinhanns, I.C.; Kappler, A.; Schoenberg, R. Iron isotope fractionation during Fe(II) oxidation
581 mediated by the oxygen-producing marine cyanobacterium *Synechococcus* PCC 7002. *Environ. Sci.*
582 *Technol.* **2017**, *51* (9), 4897-4906.

583 (32) Swanner, E.D.; Wu, W.; Schoenberg, R.; Byrne, J.; Michel, F.M.; Pan, Y.; Kappler, A.
584 Fractionation of Fe isotopes during Fe(II) oxidation by a marine photoferotroph is controlled by the
585 formation of organic Fe-complexes and colloidal Fe fractions. *Geochim. Cosmochim. Acta* **2015**,
586 *165*, 44-61.

587 (33) Amor, M.; Busigny, V.; Louvat, P.; Tharaud, M.; Gelabert, A.; Cartigny, P.; Carlut, J.;
588 Isambert, A.; Durand-Dubief, M.; Ona-Nguema, G.; Alphantery, E.; Chebbi, I.; Guyot, F. Iron uptake
589 and magnetite biomineralization in the magnetotactic bacterium *Magnetospirillum magneticum* strain
590 AMB-1: An iron isotope study. *Geochim. Cosmochim. Acta* **2018**, *232*, 225-243.

591 (34) Zhou, Z.; Latta, D.E.; Noor, N.; Thompson, A.; Borch, T.; Scherer, M.M. Fe(II)-catalyzed
592 transformation of organic matter-ferrihydrite coprecipitates: A closer look using Fe isotopes. *Environ.*
593 *Sci. Technol.* **2018**, *52*, 11142-11150.

594 (35) Brantley, S.L.; Liermann, L.J.; Gynn, R.L.; Anbar, A.; Icopini, G.A.; Barling, J. Fe isotopic
595 fractionation during mineral dissolution with and without bacteria. *Geochim. Cosmochim. Acta* **2004**,
596 *68*, 3189-3204.

597 (36) Crosby, H.A.; Johnson, C.M.; Roden, E.E.; Beard, B.L. Coupled Fe(II)-Fe(III) electron and
598 atom exchange as a mechanism for Fe isotope fractionation during dissimilatory iron oxide reduction.
599 *Environ. Sci. Technol.* **2005**, *39*, 6698-6704.

600 (37) Ilina, S.M.; Poitrasson, F.; Lapitskiy, S.A.; Alekhin, Yu.V.; Viers, J.; Pokrovsky, O.S. Extreme
601 iron isotope fractionation between colloids and particles of boreal and temperate organic-rich waters.
602 *Geochim. Cosmochim. Acta* **2013**, *101*, 96-111.

603 (38) Kopáček, J.; Maresova, M.; Norton, S.A.; Porcal, P.; Vesely, J. Photochemical source of metals
604 for sediments. *Environ. Sci. Technol.* **2006**, *40*, 4455-4459.

605 (39) Wu, L.L.; Beard, B.L.; Roden, E.E.; Johnson, C.M. Stable iron isotope fractionation between
606 aqueous Fe(II) and hydrous ferric oxide. *Environ. Sci. Technol.* **2011**, *45* (5), 1847-1852.

607 (40) Skulan, J.L.; Beard, B.L.; Johnson, C.M. Kinetic and equilibrium Fe isotope fractionation
608 between aqueous Fe(III) and hematite. *Geochim. Cosmochim. Acta* **2002**, *66*, 2995-3015.

609 (41) Frierdich, A.J.; Beard, B.L.; Reddy, T.R.; Scherer, M.M.; Johnson, C.M. Iron isotope
610 fractionation between aqueous Fe(II) and goethite revisited: New insights based on a multi-direction
611 approach to equilibrium and isotopic exchange rate modification. *Geochim. Cosmochim. Acta* **2014**,
612 *139*, 383-398.

613 (42) Sun, R.Y.; Wang, B.L. Iron isotope fractionation during uptake of ferrous ion by phytoplankton.
614 *Chem. Geol.* **2018**, *481*, 65-73.

615 (43) Vasyukova, E.V.; Pokrovsky, O.S.; Viers, J.; Oliva, P.; Dupré, B.; Martin, F.; Candadaup, F. Trace
616 elements in organic- and iron-rich surficial fluids of the boreal zone: Assessing colloidal forms via dialysis
617 and ultrafiltration. *Geochim. Cosmochim. Acta* **2010**, *74*, 449-468.

618 (44) González, A.G.; Pokrovsky, O.S.; Jimenez-Villacorta, F.; Shirokova, L.S.; Santana-Casiano, J.M.;
619 González-Davila, M.; Emnova, E.E. Iron adsorption onto soil and aquatic bacteria: XAS structural study.
620 *Chem. Geol.* **2014**, *372*, 32-45

621 (45) Viollier, E.; Inglett, P.W.; Hunter, K.; Roychoudhury, A.N.; Van Cappellen, P. The ferrozine
622 method revisited: Fe(II)/Fe(III) determination in natural waters. *Appl. Geochem.* **2000**, *15* (6), 785-
623 790.

- 624 (46) Mulholland, D.S.; Poitrasson, F.; Boaventura, G.R.; Allard, T.; Vieira, L.C.; Santos, R.V.;
625 Mancini, L.; Seyler, P. Insights into iron sources and pathways in the Amazon River provided by
626 isotopic and spectroscopic studies. *Geochim. Cosmochim. Acta* **2015**, *150*, 142-159.
- 627 (47) Ilina, S.M.; Drozdova, O.Y.; Lapitsky, S.A.; Alekhin, Yu.V.; Demin, V.V.; Zavgorodnaya,
628 Yu.A.; Shirokova, L.S.; Viers, J.; Pokrovsky, O.S. Size fractionation and optical properties of
629 dissolved organic matter in the continuum soil solution-bog-river and terminal lake of a boreal
630 watershed. *Organic Geochem.* **2014**, *66*, 14–24.
- 631 (48) Gustafsson, J. Visual MINTEQ ver. 3.1. <http://vminteq.lwr.kth.se>, 2014, assessed 8.02.2019.
- 632 (49) Poitrasson F.; Freyrier, R. Heavy iron isotope composition of granites determined by high
633 resolution MC-ICP-MS. *Chem. Geol.* **2005**, *222*, 132–147.
- 634 (50) Mulholland, D.S.; Poitrasson, F.; Boaventura, G.R. Effect of different water storage procedures
635 on the dissolved Fe concentration and isotopic composition of chemically contrasted waters from the
636 Amazon River Basin. *Rapid Comm. Mass Spectr.* **2015**, *29*, 2102-2108.
- 637 (51) Kafantaris, F.C.A.; Borrok, D.M. Zinc isotope fractionation during surface adsorption and
638 intracellular incorporation by bacteria. *Chem. Geol.* **2014**, *366*, 42–51.
- 639 (52) Croal, L.R.; Johnson, C.M.; Beard, B.L.; Newman, D.K. Iron isotope fractionation by Fe(II)-
640 oxidizing photoautotrophic bacteria. *Geochim. Cosmochim. Acta* **2004**, *68*, 1227-1242.
- 641 (53) Bullen, T.D.; White, A.F.; Childs, C.W.; Vivit, D.V.; Schulz, M.S. Demonstration of
642 significant abiotic iron isotope fractionation in nature. *Geology* **2001**, *29*, 699-702.
- 643 (54) Beard, B.L.; Handler, R.M.; Scherer, M.M.; Wu, L.; Czaja, A.D.; Heimann, A.; Johnson, C.M.
644 Iron isotope fractionation between aqueous ferrous iron and goethite. *Earth Planet. Sci. Lett.* **2010**,
645 *295* (1-2), 241-250.
- 646 (55) Dideriksen, K.; Baker, J.A.; Stipp, S.L.S. Equilibrium Fe isotope fractionation between
647 inorganic aqueous Fe(III) and the siderophore complex, Fe(III)-desferrioxamine B. *Earth Planet. Sci.*
648 *Lett.* **2008**, *269*, 280- 290.
- 649 (56) Morgan, J. L.; Wasylenki, L. E.; Nuester, J.; Anbar, A. D. Fe isotope fractionation during
650 equilibration of Fe-organic complexes. *Environ. Sci. Technol.* **2010**, *44*, 6095–6101.
- 651 (57) Chupakova, A.A.; Chupakov, A.V.; Neverova, N.V.; Shirokova, L.S.; Pokrovsky, O.S.
652 Photodegradation of river dissolved organic matter and trace metals in the largest European Arctic
653 estuary. *Sci. Total Environ.* **2018**, *622–623*, 1343–1352.
- 654 (58) Barbeau, K.; Rue, E.; Bruland, K.; Butler A. Photochemical cycling of iron in the surface ocean
655 mediated by microbial iron (III)-binding ligands. *Nature* **2001**, *413*, 409–413.
- 656 (59) Welch, S.A.; Beard, B.L.; Johnson, C.M.; Braterman, P.S. Kinetic and equilibrium Fe isotope
657 fractionation between aqueous Fe(II) and Fe(III). *Geochim. Cosmochim. Acta* **2003**, *67*(22), 4231–
658 4250.
- 659 (60) Balci, N.; Bullen, T.D.; Witte-Lien, K.; Shanks, W.C.; Motelica, M.; Mandernack, K.W. Iron
660 isotope fractionation during microbially stimulated Fe(II) oxidation and Fe(III) precipitation.
661 *Geochim. Cosmochim. Acta* **2006**, *70*, 622–639.
- 662 (61) Teutsch, N.; Von Gunten, U.; Porcelli, D.; Cirpka, O.A.; Halliday, A.N. Adsorption as a cause
663 for iron isotope fractionation in reduced groundwater. *Geochim. Cosmochim. Acta* **2005**, *69*(17), 4175–
664 4185.
- 665 (62) Johnson, C.M.; Beard, B.L.; Roden, E.E.; Newman, D.K.; Neelson, K.H. Isotopic constraints
666 on biogeochemical cycling of Fe. *Rev. Mineral. Geochem.* **2004**, *55*, 359–408.
- 667 (63) Reddy, T.R.; Friedrich, A.J.; Beard, B.L.; Johnson, C.M. The effect of pH on stable iron
668 isotope exchange and fractionation between aqueous Fe(II) and goethite. *Chem. Geol.* **2015**, *397*, 118–
669 127.
- 670 (64) Handler, R.M.; Beard, B.L.; Johnson, C.M.; Scherer, M.M. Atom exchange between
671 aqueous Fe(II) and goethite: an Fe isotope tracer study. *Environ. Sci. Technol.* **2009**, *43*(4), 1102–
672 1107.
- 673 (65) Voelker, B.M.; Sulzberger, B. Effects of fulvic acid on Fe(II) oxidation by hydrogen peroxide.
674 *Environ. Sci. Technol.* **1996**, *30*, 1106-1114.

675 (66) Anesio, A.M.; Granéli, W. Increased photoreactivity of DOC by acidification: Implication for
676 the carbon cycle in humic lakes. *Limnol. Oceanogr.* **2003**, *48*, 735–744.

677 (67) Gao, H.; Zepp, R.G. Factors influencing photoreactions of dissolved organic matter in a coastal
678 river of the southeastern United States. *Environ. Sci. Technol.* **1998**, *32*, 2940–2946.

679 (68) Wang, Y.; Xiang, W.; Yang, W.; Yan, S.; Bao, Z.; Liu, Y. Photo-stability of iron-phenolic
680 complexes derived from peatland upon irradiation in waters under simulated sunlight. *Chem. Geol.*
681 **2018**, *485*, 14-23.

682 (69) Helms, J.R.; Mao, J.; Schmidt-Rohr, K.; Abdulla, H.; Mopper, K. Photochemical flocculation
683 of terrestrial dissolved organic matter and iron. *Geochim. Cosmochim. Acta* **2013**, *121*, 398–413.

684 (70) Catrouillet, C.; Davranche, M.; Dia, A.; Bouhnik-Le Coz, M.; Marsac, R.; Pourret, O.; Gruau,
685 G. Geochemical modeling of Fe(II) binding to humic and fulvic acids. *Chemical Geol.* **2014**, *372*, 109-
686 118.

687 (71) Dauphas, N.; John, S.G.; Rouxel, O. Iron isotope systematics. *Rev. Mineral. Geochem.* **2017**,
688 *82*, 415-510.

689 (72) Drozdova, O.Yu.; Ilina, S.M.; Lapitsky, S.A. The transformation of dissolved organic matter
690 in the soil water - bog - stream - terinal lake continuum of a boreal watershed (Northern Karelia), in:
691 Pokrovsky, O.S., Shirokova, L.S., eds. *Dissolved Organic Matter (DOM): Properties, Applications*
692 *and Behavior*, Nova Publishers, N.Y., 2017, pp. 115-133.

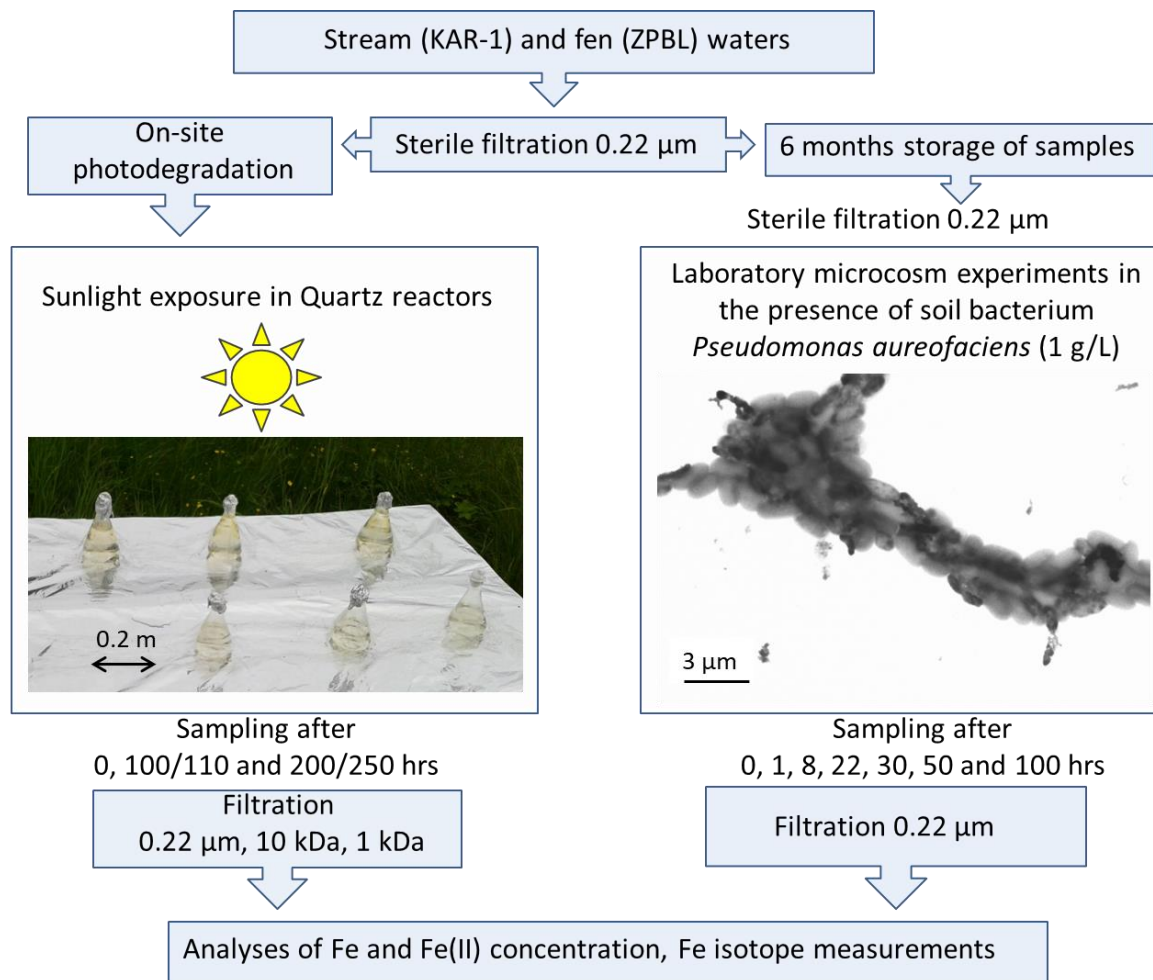
693
694
695
696
697
698
699
700
701
702
703
704
705
706
707
708
709
710
711
712
713
714
715
716
717
718
719
720
721
722
723
724
725
726

727
728
729
730
731
732
733
734
735

Table 1. Measured pH, DOC, Fe concentrations and isotopic ratios, relative to IRMM-14, during bio- and photo-degradation experiments. Note that the DOC in biodegradation experiments of stream water slightly increased due to cell lysis and exometabolite production. The standard error was calculated using the Student's t factor: $SE = (t \times SD) / \sqrt{N}$, where N is the number of measurements.

Bio-degradation (1 g _{wet} /L of <i>Pseudomonas aureofaciens</i>)											
hrs	Fen water ZPBL <0.22 µm					hrs	Stream water KAR-1 <0.22 µm				
	pH	DOC, mg L ⁻¹	Fe, µg L ⁻¹	Fe(II), µg L ⁻¹	δ ⁵⁷ Fe ±2 SE, ‰		pH	DOC, mg L ⁻¹	Fe, µg L ⁻¹	Fe(II), µg L ⁻¹	δ ⁵⁷ Fe ±2 SE, ‰
0	4.9	37.4	2470±45	645±20	1.06±0.05	0	6.6	12.4	180±10	30±20	2.87±0.07
1	5.2	37.0	1690±20	620±20	0.86±0.07	1	6.4	13.6	115±7	< LOQ*	2.54±0.06
8	5.4	35.8	1520±20	290±10	0.85±0.12	8	6.4	13.0	82±10	< LOQ*	2.68±0.16
22	5.7	34.8	1365±15	no data	0.88±0.07	22	6.7	14.0	63±3	< LOQ*	3.21±0.15
30	5.8	26.6	1290±5	145±5	0.99±0.10	50	7.0	14.1	56±2	< LOQ*	3.26±0.13
50	5.8	23.3	1197±5	120±10	1.03±0.05	100	7.2	15.2	50±2	< LOQ*	no data
100	6.1	25.2	1054±5	84±5	1.04±0.04						
Sunlight exposure											
hrs	Fen water ZPBL <0.22 µm					hrs	Stream water KAR-1 <0.22 µm				
0	5.4	38.7	4310±100	840±50	0.25±0.07	0	7.2	11.9	208±20	50±20	1.59±0.05
100	5.1	20.3	1840±400	770±170	-0.8±0.38	110	6.8	10.4	193±25	60±25	1.75±0.2
200	5.3	18.7	915±30	450±10	-2.63±0.03	250	6.7	8.2	175±25	15±5	2.1±0.12
hrs	Fen water ZPBL <10 kDa					hrs	Stream water KAR-1 <10 kDa				
0	5.3	26.5	1125±50	620±20	0.19±0.02	0	6.8	10.2	35±5	20±10	2.93±0.06
100	5.2	18.7	1000±50	510±20	-1.98±0.13	110	6.9	10.0	49±10	30±20	1.95±0.06
200	5.3	17.9	945±50	470±30	-2.49±0.15	250	6.8	8.1	14±2	< LOQ*	1.89±0.07
hrs	Fen water ZPBL <1 kDa					* Limit of quantification					
0	5.6	10.6	200±20	70±10	-0.18±0.03						
100	5.3	11.5	560±30	300±100	-2.34±0.11						
200	5.4	16.8	620±30	340±100	-2.43±0.12						

736
737
738
739
740
741
742
743
744



745

746

747

748

749

750

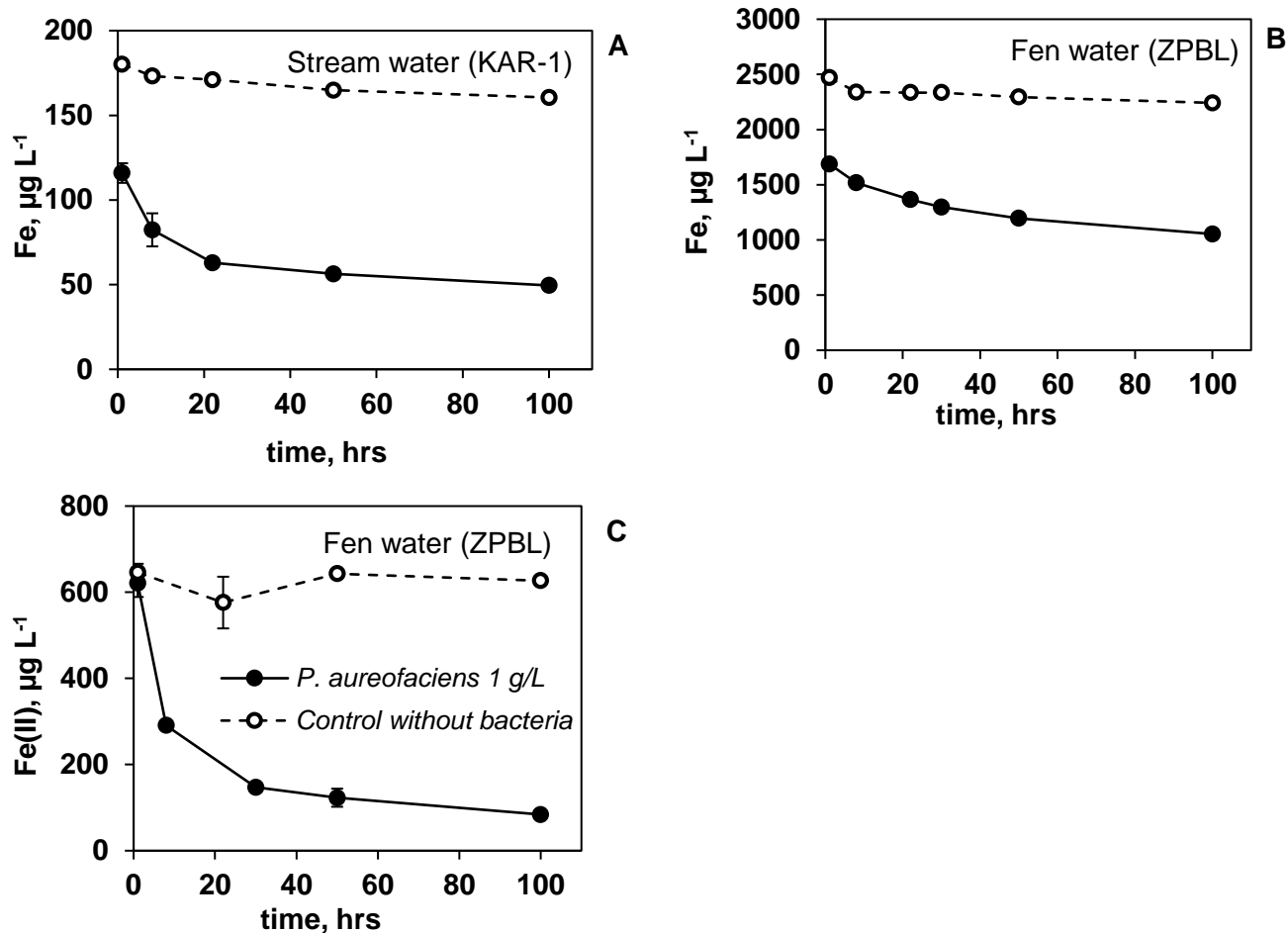
751

752

753

754

Fig. 1. Conceptual scheme of experiments (run in duplicates): a photo of quartz reactors exposed to sunlight and a Transmission Electron Microscopy (TEM) image of bacterial cells with precipitated Fe hydroxides. The photodegradation experiments were performed on-site, immediately after water sampling and sterile filtration. The biodegradation experiments required sterile laboratory environments and were run after 6 months of water storage. The biodegradation experiments included only < 0.22 μm filtration after sampling. In photodegradation experiments, the stream water was processed for the < 0.22 μm and the < 10 kDa filtration and the fen water was filtered through 0.22 μm, 10 kDa and 1 kDa.



755 **Fig. 2.** Evolution of total dissolved Fe concentration during biodegradation experiments of stream (A)
 756 and fen (B) water. (C): Fe(II) concentration evolution in the fen water during biodegradation.
 757 The error bars of biotic experiments represent 1 SD of duplicates. In most cases, they are
 758 smaller than the symbol size. Bacterial experiments are shown by solid circles and bacteria-
 759 free control is represented by open circles for all three panels as indicated in (C).

760

761

762

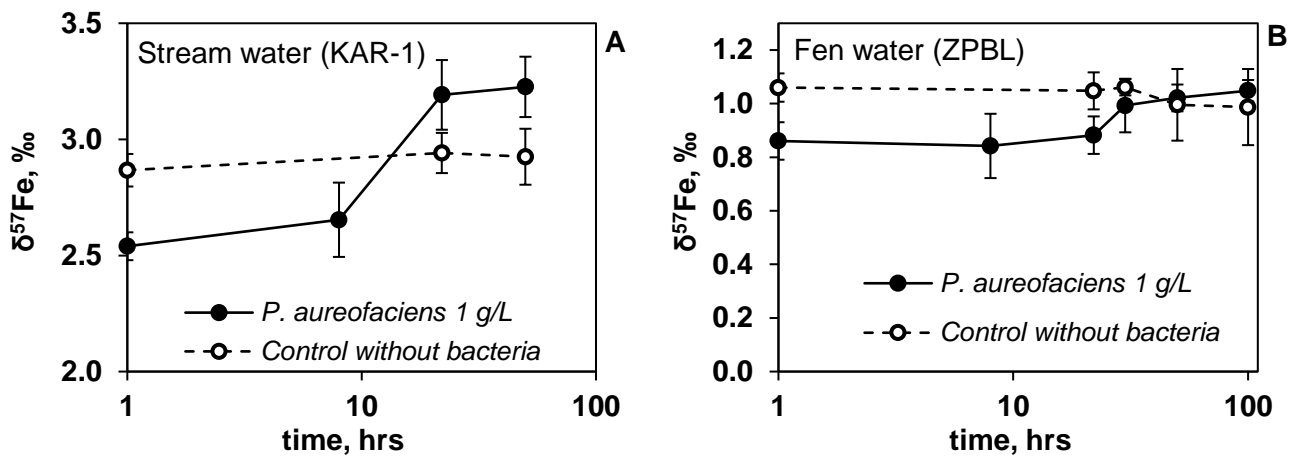
763

764

765

766

767



768

769 **Fig. 3.** Evolution of isotopic ratios $\delta^{57}\text{Fe}$ during biodegradation experiments of stream (A) and fen (B)
770 water. Note log scale for time axis..

771

772

773

774

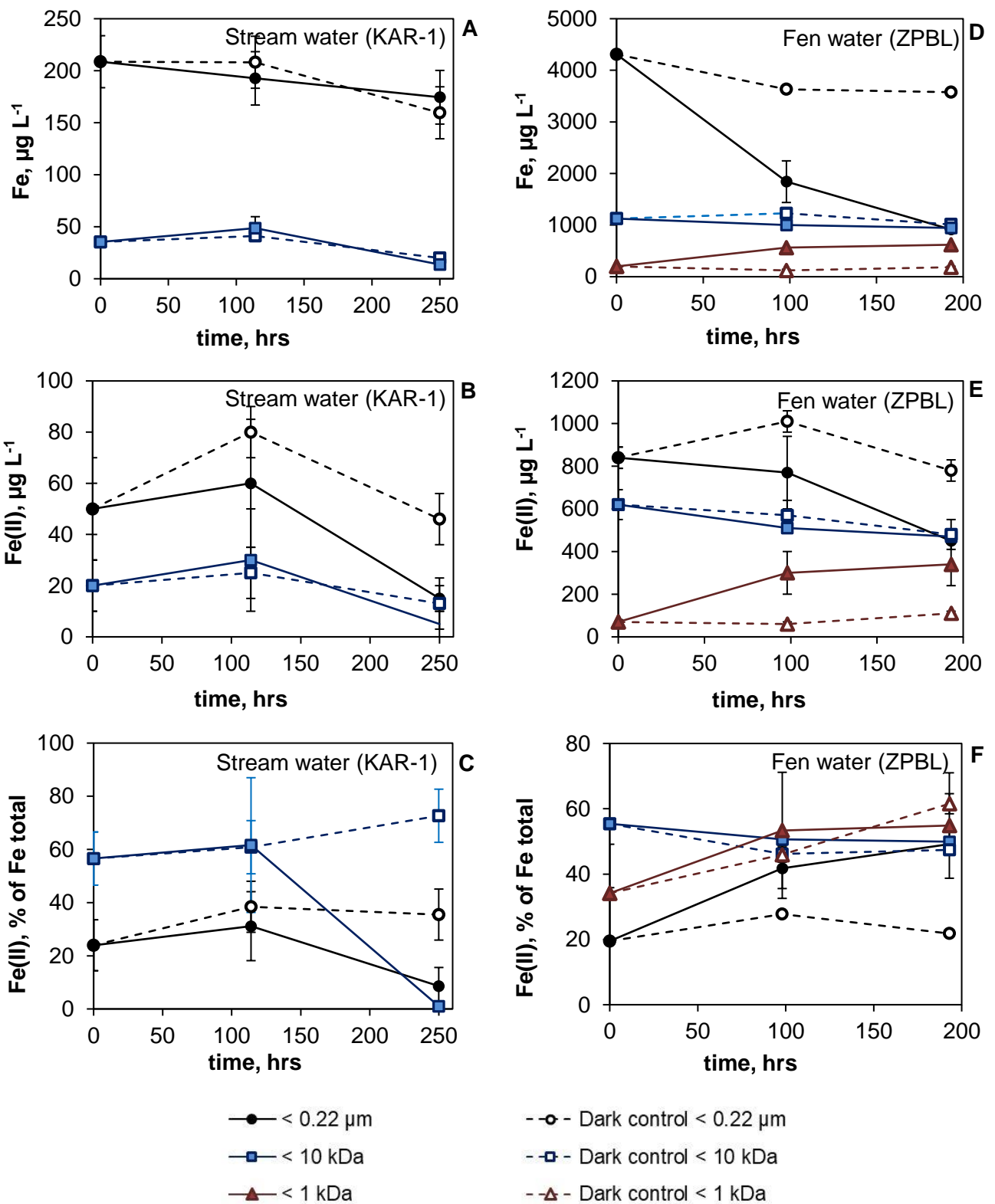
775

776

777

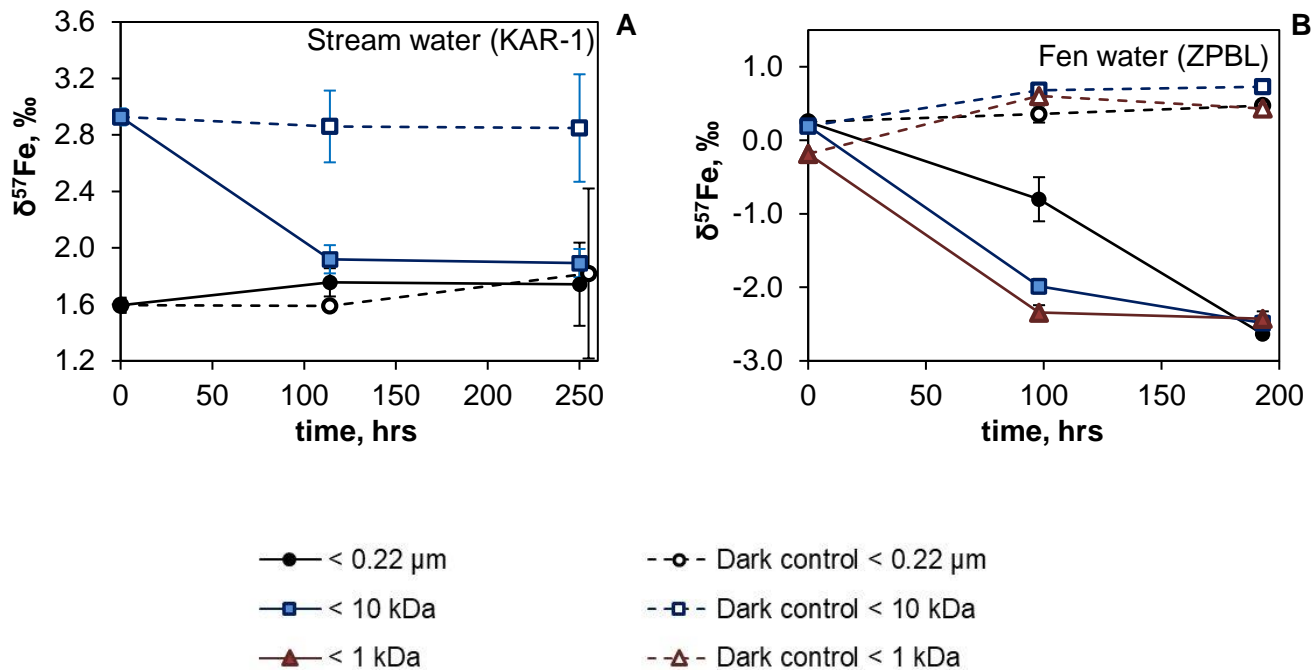
778

779



780 **Fig. 4.** Evolution of Fe_{tot} and Fe(II) concentration during photodegradation experiments of
 781 stream (A, B, C) and fen (D, E and F) water in quartz reactors. Note a drop in Fe_{tot} and Fe(II)
 782 concentration of the < 0.22 μm dark control at 200 and 250 h not observed in previously stored samples
 783 in biodegradation experiments (Fig. 2), which may be due to partial coagulation of freshly sampled
 784 natural water upon storage.

785
786



787

788 **Fig 5.** Evolution of isotopic ratios $\delta^{57}\text{Fe}$ during photodegradation experiments of stream (A) and fen
789 (B) water. There is a clear decrease in $\delta^{57}\text{Fe}$ value in all fractions of photodegraded samples
790 of fen water, but this decrease is only pronounced for the < 10 kDa fraction of stream water.
791 Note that a weak increase in $\delta^{57}\text{Fe}$ for the < 0.22 μm dark control in KAR-1 is within the
792 uncertainty of replicates. An increase in $\delta^{57}\text{Fe}$ for the < 1 kDa and < 10 kDa dark control of
793 fen waters is due to Fe loss of these unstable, freshly sampled waters.

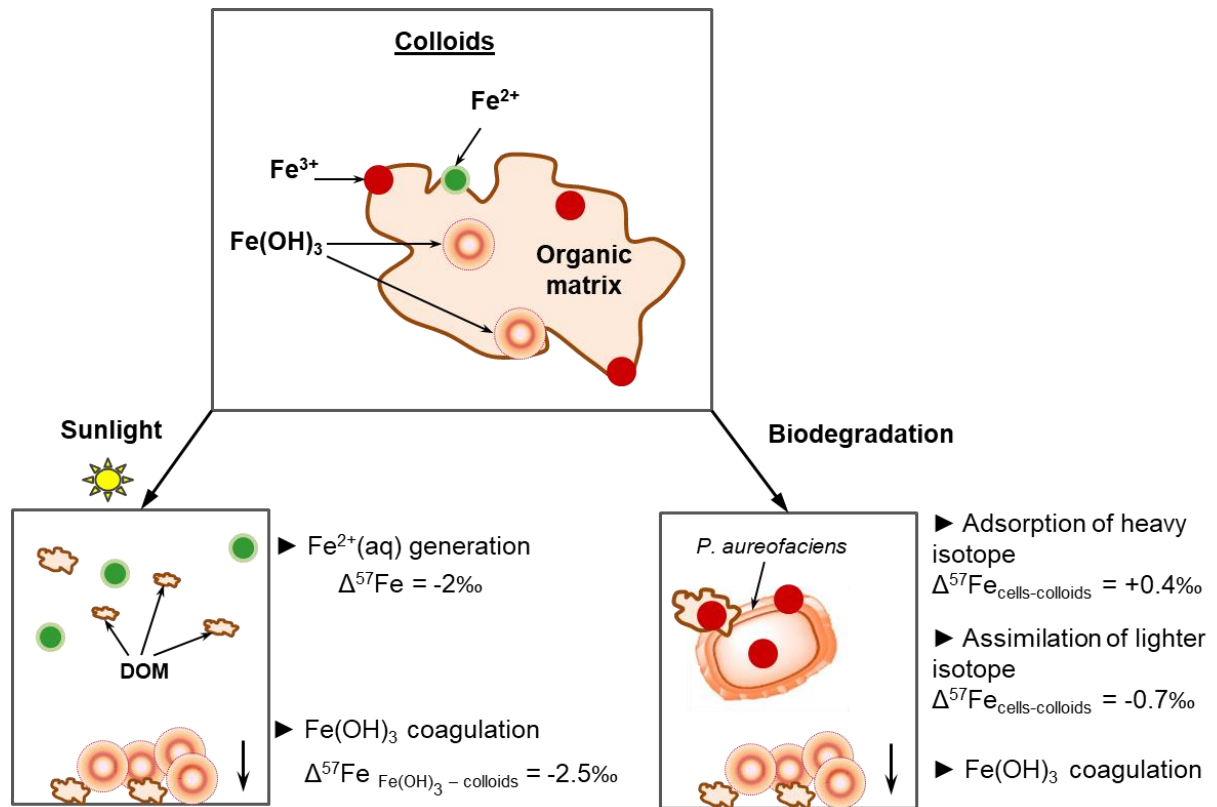
794

795

796

797

798



799

800 **Fig. 6.** Cartoon of Fe isotope fractionation under sunlight-induced transformation (left) and
 801 biodegradation (right) of organic and organo-ferric colloids (1 kDa - 0.22 μ m). Live heterotrophic *P.*
 802 *aureofaciens* bacteria adsorb heavier and assimilate lighter Fe isotopes. Sunlight irradiation
 803 generates isotopically light Fe(II) in low molecular weight (< 1 kDa) fraction and produces heavy
 804 isotope enrichment in particulate fraction relative to total dissolved (< 0.22 μ m) form. After bio- or
 805 photo-degradation of organic matter which constitutes organo-ferric colloids, the liberation of Fe(III)
 806 ions and precipitation of Fe(III) hydroxide occur. This removes heavier isotopes from solution into
 807 the solid phase. Altogether, bio- and photodegradation of organo-ferric colloids can produce very Fe)
 808 large, from -2 to +3‰ isotopic variations ($\delta^{57}Fe$) in boreal humic waters.
 809